Cellular Oncology (2025) 48:655–671
https://doi.org/10.1007/s13402-025-01038-9

RESEARCH

LPA released from dying cancer cells after chemotherapy inactivates Hippo signaling and promotes pancreatic cancer cell repopulation

Yuzhi Liu[1] · Jie Ding[1] · Shumin Li[2] · Anyi Jiang[1] · Zhiqin Chen[1] · Ming Quan[1]

Accepted: 9 January 2025 / Published online: 4 February 2025

Abstract

Purpose The Hippo pathway in the tumorigenesis and progression of PDAC, with lysophosphatidic acid (LPA) regulating the Hippo pathway to facilitate cancer progression. However, the impact of the Hippo signaling pathway on tumor repopulation in PDAC remains unreported.

Methods Direct and indirect co-culture models to investigate gemcitabine-induced apoptotic cells can facilitate the repopulation of residual tumor cells. Mass spectrometry analysis was conducted to assess the impact of gemcitabine treatment on the lipid metabolism of pancreatic cancer cells. ELISA assays confirmed gemcitabine promotes the release of LPA from apoptotic pancreatic cancer cells. The expression of Yes-associated protein 1 (*YAP1*) elucidated the underlying mechanism by which dying cells induce tumor repopulation using RT-qPCR and Western blot. We studied the biological function of pancreatic cancer cells using CCK-8, colony formation, and transwell invasion assays in vitro. Co-culture models were used to validate the impact of Hippo pathway on tumor repopulation, while flow cytometry was employed to assess the sensitivity of pancreatic cancer cells to gemcitabine in the context of Hippo pathway.

Results Gemcitabine-induced dying cells released LPA in a dose-dependent manner, which promoted the proliferation, clonal formation, and invasion of pancreatic cancer cells. Mechanistic studies showed that gemcitabine and LPA facilitated the translocation of *YAP1* and induced the inactivation of the Hippo pathway. *YAP1* overexpression significantly enhanced the activity of autotaxin, leading to stimulated pancreatic cancer cells to secrete LPA. This mechanism orchestrated a self-sustaining LPA-Hippo feedback loop, which drove the repopulation of residual tumor cells. Simultaneously, it was observed that suppressing LPA and *YAP1* expression enhanced the sensitivity of pancreatic cancer cells to gemcitabine.

Conclusion Our investigation indicated that targeting the LPA-*YAP1* signaling pathway could serve as a promising strategy to augment the overall therapeutic efficacy against PDAC.

Keywords PDAC · Tumor repopulation · LPA · Hippo signaling

Yuzhi Liu, Jie Ding and Shumin Li contributed equally.

✉ Zhiqin Chen
18240266409@163.com

✉ Ming Quan
mquan@tongji.edu.cn

Yuzhi Liu
liuyuzhi9808@163.com

Jie Ding
ding_23@163.com

Shumin Li
lishumin94@163.com

Anyi Jiang
jaydoct@163.com

[1] Department of Oncology, Shanghai East Hospital, Tongji University School of Medicine, Shanghai 200123, China

[2] Department of Oncology and State Key Laboratory of Systems Medicine for Cancer of Shanghai Cancer Institute, Renji Hospital, School of Medicine, Shanghai Jiaotong University, Shanghai 200127, China

Abbreviations

PDAC	Pancreatic ductal adenocarcinoma
LPC	Lysophosphatidylcholine
LPA	Lysophosphatidic acid
TG	Triglyceride
PE	Phosphatidylinositol
iPLA2	Calcium-independent phospholipase A2
AA	Arachidonic acid
PGE2	Prostaglandin E2
LC-MS/MS	Liquid chromatography-tandem mass spectrometry
UMI	Unique molecular identifier
RPMI	Roswell park memorial institute
FBS	Fetal bovine serum
RT-qPCR	Real time quantitative polymerase chain reaction
GSEA	Gene set enrichment analysis
PCA	Principal component analysis
CCK-8	Cell Counting Kit-8
ANOVA	Analysis of variance
IC50	Half-maximal inhibitory concentration
Mt	Mitochondrial
Rb	Ribosomal
HSA	Highest Single Agent
GPCRs	G-protein-coupled receptors
GO	Gene Ontology
KEGG	Kyoto Encyclopedia of Genes and Genomes
TME	Tumor microenvironment
scRNA-seq	Single-cell RNA sequencing
ATX	Autotaxin
YAP1	Yes-associated protein 1
TEAD	Transcriptional enhanced associate domain
MST1/2	Mammalian Sterile 20-like kinase 1/2
LATS1/2	Large tumor suppressor 1/2
IL6	Interleukin 6
IL8	Interleukin 8
SREBP2	Sterol regulatory element-binding protein-2
FASN	Fatty acid synthase

1 Introduction

Pancreatic ductal adenocarcinoma (PDAC) is among the leading causes of cancer-related mortality worldwide, with an overall survival rate of less than 5%. Gemcitabine-based chemotherapy is the standard treatment for locally advanced or unresectable PDAC cases [1, 2]. However, drug resistance frequently occurs during chemotherapy. As one of the reasons for the occurrence of drug resistance, tumor repopulation plays a critical role in therapeutic failure. It has been reported that tumor cells surviving chemoradiotherapy could repopulate during treatment intervals [3]. Emerging evidence suggests that dying cells can drive the repopulation of pancreatic cancer cells through signaling pathways involving Hedgehog, Wnt, and the microRNA-193a-TGF-β2 signaling axis [4–6]. Furthermore, caspase-3 regulates prostaglandin E2 (PGE2) to foster the proliferation of surviving tumor cells, suggesting the existence of a cell death-mediated tumor repopulation pathway [7]. Despite these findings, the precise mechanisms underlying this process remain unclear.

The Hippo pathway plays a crucial role in various human cancers, including PDAC. When the Hippo pathway is deactivated, Yes-associated protein 1 (*YAP1*)/*TAZ* undergo dephosphorylation and translocate to the nucleus, where they interact with transcriptional enhanced associate domain (*TEAD*) to drive tumorigenic processes [8, 9]. Alterations in lipid metabolism, particularly lysophosphatidic acid (LPA) receptor-mediated signaling, profoundly influence cancer cell behavior and promote tumor progression [10]. Autotaxin (*ATX*), a secreted enzyme highly expressed in PDAC, catalyzes conversion of lysophosphatidylcholine (LPC) into LPA [11]. LPA, in turn, can inhibit large tumor suppressor 1/2 (*LATS1/2*) via G12/13-coupled receptors, thereby activating the transcriptional co-activator *YAP1* [12]. However, the role of the *ATX*-LPA axis in the repopulation of pancreatic cancer remains insufficiently explored.

In this study, we investigated the hypothesis that dying pancreatic cancer cells may provide initial signals that drive tumor repopulation following chemotherapy. Specifically, we demonstrated that gemcitabine induces dying pancreatic cancer cells to release LPA, which subsequently mediates Hippo pathway inactivation. Additionally, we identified a positive feedback loop between LPA and *YAP1*. Targeting the LPA-*YAP1* axis may offer an effective strategy to overcome chemoresistance in PDAC.

2 Results

2.1 Gemcitabine promotes the repopulation of residual tumor cells in vitro

To assess the repopulation of residual PDAC cells following gemcitabine treatment, we first determined the half-maximal inhibitory concentration (IC50) value of gemcitabine using a Cell Counting Kit-8 (CCK-8) assay. The results revealed that the IC50 values for the PDAC cell lines were approximately 1 μM (Fig. 1A).

Subsequently, we investigated whether dying cells could facilitate the repopulation of residual pancreatic cancer cells using both direct and indirect co-culture models (Fig. 1B). Results from these models showed that gemcitabine-treated dying cells significantly enhanced the proliferation activity

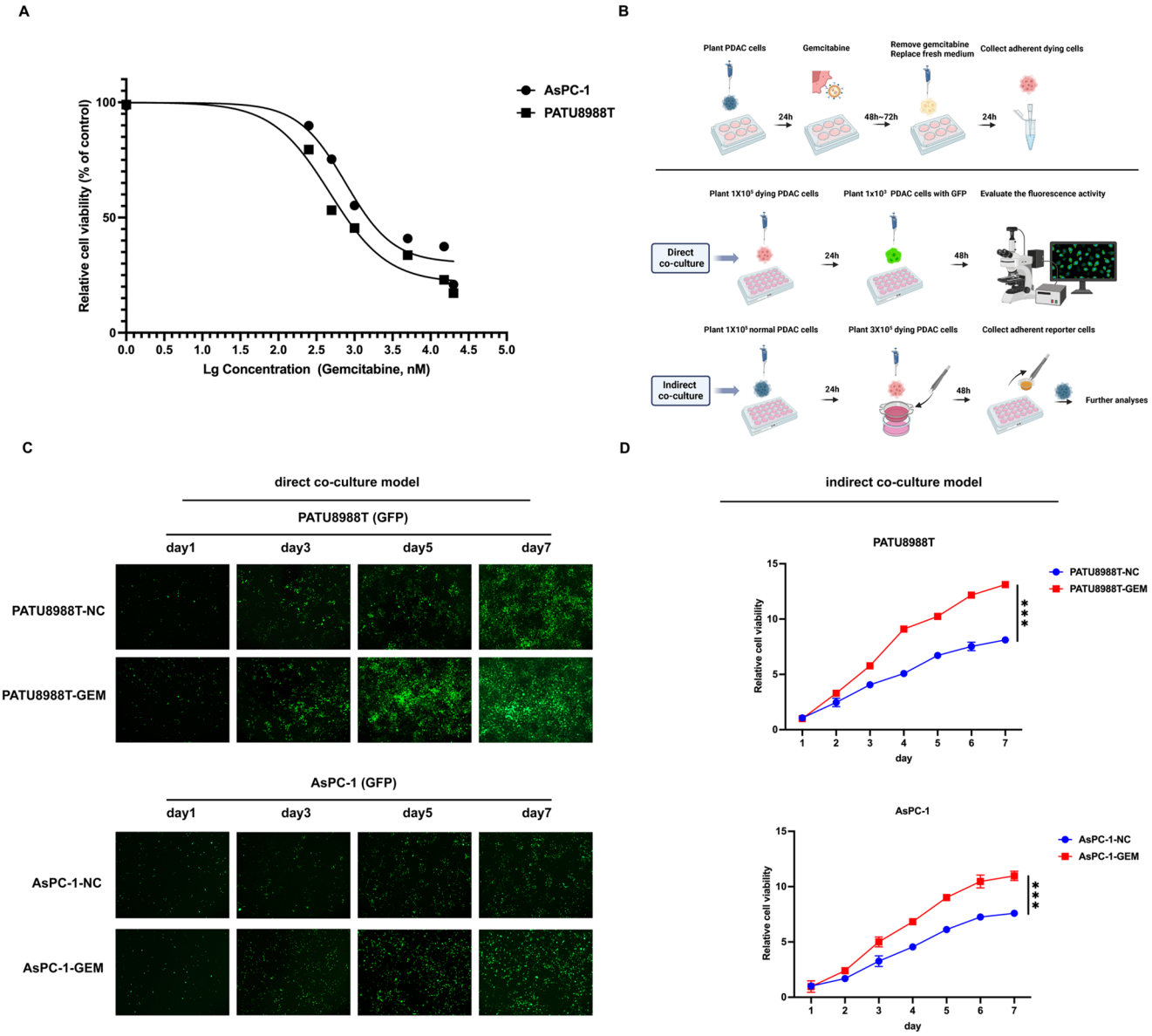

Fig. 1 Gemcitabine promotes the repopulation of residual tumor cells in vitro. **A** The half-maximal inhibitory concentration (IC50) of gemcitabine for PATU8988T and AsPC-1 cell lines was determined using the CCK-8 assay. **B** Schematic illustration of the direct and indirect co-culture models used in this study. **C** Proliferative activity of reporter cells in the direct co-culture model was assessed by fluorescence intensity. In the gemcitabine-treated (GEM) group, dying cells were treated with 1~5 μM gemcitabine, whereas in the negative control (NC) group, pancreatic cancer cells were treated with DMSO. **D** Proliferative capacity of reporter cells in the indirect co-culture model was evaluated using the CCK-8 assay. All experiments were performed in biological triplicates, and data are presented as the mean ± standard deviation. Statistical significance was determined by $^{*}P < 0.05$, $^{**}P < 0.01$, and $^{***}P < 0.001$

of reporter cells (Fig. 1C and D). Collectively, our findings indicate that gemcitabine-treated dying cells could promote the repopulation of residual pancreatic cancer cells.

2.2 Gemcitabine induces LPA release and Hippo pathway inactivation in PDAC

Using the UPLC-MS/MS detection platform, we performed a lipid metabolomics analysis to investigate lipid alterations. Compared to the control group, gemcitabine treatment led to significant upregulation of various lipids, including triglycerides (TG), phosphatidylinositol (PE), cholesterol, and LPA (Fig. 2A). Our previous studies demonstrated that caspase-3 can promote tumor cell regeneration through its effects on Calcium-independent phospholipase A2 (iPLA2). Notably, the role and mechanism of the iPLA2 - AA (arachidonic acid) - PGE2 signal axis have been thoroughly examined in the context of tumor repopulation [7, 13].

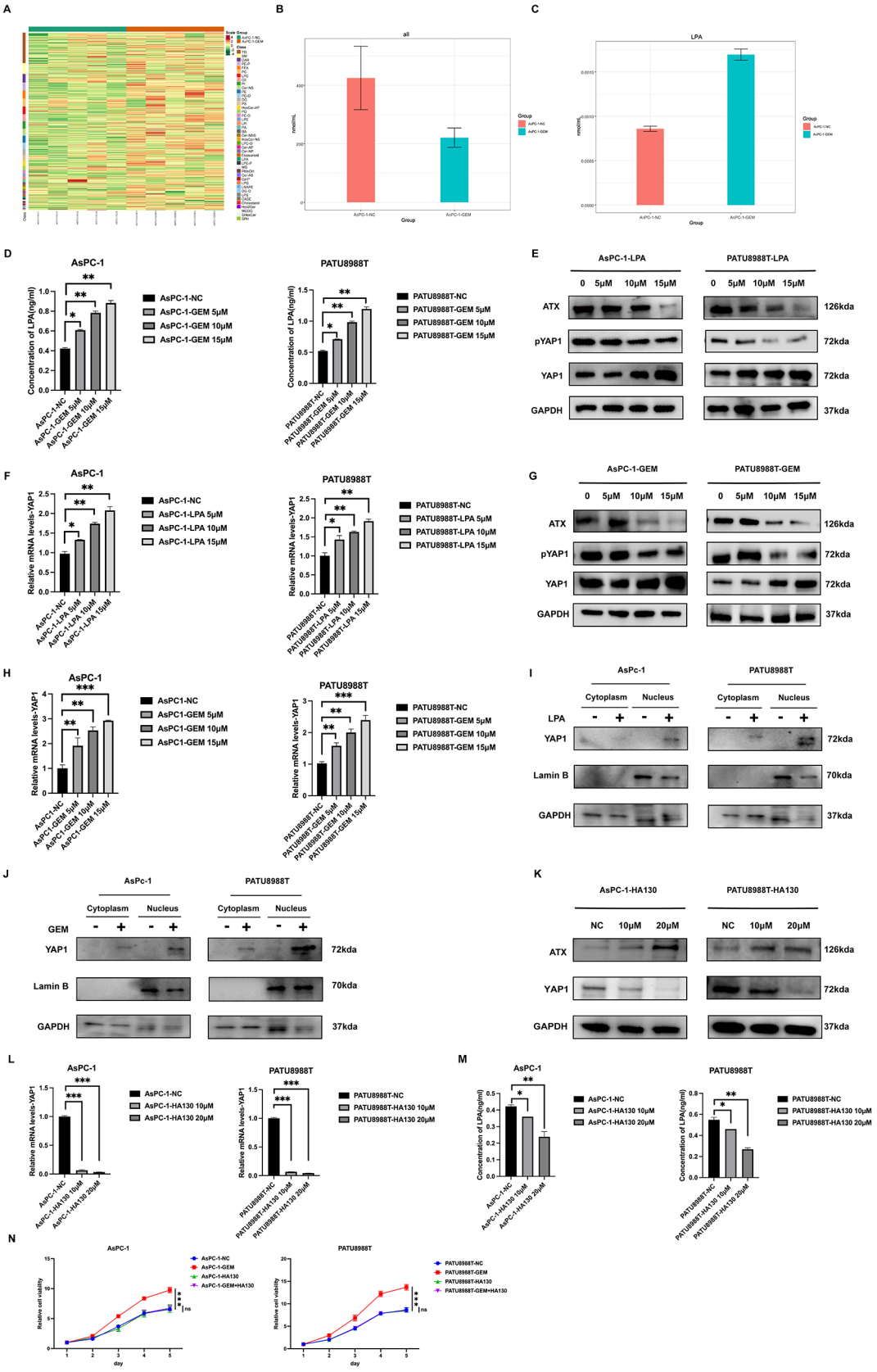
A
B
all
nmol/mL
Group
AsPC-1-NC
AsPC-1-GEM
C
LPA
nmol/mL
Group
D
AsPC-1
Concentration of LPA(ng/ml)
AsPC-1-NC
AsPC-1-GEM 5μM
AsPC-1-GEM 10μM
AsPC-1-GEM 15μM
PATU8988T
PATU8988T-NC
PATU8988T-GEM 5μM
PATU8988T-GEM 10μM
PATU8988T-GEM 15μM
E
AsPC-1-LPA
PATU8988T-LPA
0 5μM 10μM 15μM
ATX
pYAP1
YAP1
GAPDH
126kda
72kda
72kda
37kda
F
AsPC-1
Relative mRNA levels-YAP1
AsPC-1-NC
AsPC-1-LPA 5μM
AsPC-1-LPA 10μM
AsPC-1-LPA 15μM
PATU8988T
PATU8988T-NC
PATU8988T-LPA 5μM
PATU8988T-LPA 10μM
PATU8988T-LPA 15μM
G
AsPC-1-GEM
PATU8988T-GEM
0 5μM 10μM 15μM
ATX
pYAP1
YAP1
GAPDH
126kda
72kda
72kda
37kda
H
AsPC-1
Relative mRNA levels-YAP1
AsPC1-NC
AsPC1-GEM 5μM
AsPC1-GEM 10μM
AsPC1-GEM 15μM
PATU8988T
PATU8988T-NC
PATU8988T-GEM 5μM
PATU8988T-GEM 10μM
PATU8988T-GEM 15μM
I
AsPc-1
PATU8988T
Cytoplasm Nucleus
LPA
YAP1
Lamin B
GAPDH
72kda
70kda
37kda
J
AsPc-1
PATU8988T
Cytoplasm Nucleus
GEM
YAP1
Lamin B
GAPDH
72kda
70kda
37kda
K
AsPC-1-HA130
PATU8988T-HA130
NC 10μM 20μM
ATX
YAP1
GAPDH
126kda
72kda
37kda
L
AsPC-1
Relative mRNA levels-YAP1
AsPC-1-NC
AsPC-1-HA130 10μM
AsPC-1-HA130 20μM
PATU8988T
PATU8988T-NC
PATU8988T-HA130 10μM
PATU8988T-HA130 20μM
M
AsPC-1
Concentration of LPA(ng/ml)
AsPC-1-NC
AsPC-1-HA130 10μM
AsPC-1-HA130 20μM
PATU8988T
PATU8988T-NC
PATU8988T-HA130 10μM
PATU8988T-HA130 20μM
N
AsPC-1
Relative cell viability
day
AsPC-1-NC
AsPC-1-GEM
AsPC-1-HA130
AsPC-1-GEM+HA130
PATU8988T
PATU8988T-NC
PATU8988T-GEM
PATU8988T-HA130
PATU8988T-GEM+HA130

Fig. 2 Gemcitabine induces LPA release and Hippo pathway inactivation in PDAC. **A** Hierarchical heatmap illustrating differences in lipid classes in conditioned media between the NC and GEM groups, as determined by UPLC-MS/MS. **B** Total lipid concentrations in conditioned media of the NC and GEM groups. **C** The concentrations of LPA in conditioned media of the NC and GEM groups. **D** The ELISA assays measuring LPA levels in conditioned media post-gemcitabine treatment. **E** LPA induces *YAP1* dephosphorylation and suppresses *ATX* expression in a dose-dependent manner. **F** LPA enhances *YAP1* mRNA expression in a dose-dependent manner. **G** Gemcitabine reduces *YAP1* phosphorylation and downregulates *ATX* expression in a dose-dependent manner. **H** Gemcitabine promotes *YAP1* mRNA expression in a dose-dependent manner. **I** LPA (10 μM) induces nuclear translocation of *YAP1* in pancreatic cancer cells. **J** Gemcitabine (10 μM) facilitates nuclear translocation of *YAP1* in pancreatic cancer cells. **K** HA130 (20 μM) inhibits *YAP1* protein expression and increases *ATX* protein expression in pancreatic cancer cells. **L** HA130 (20 μM) significantly reduces *YAP1* mRNA expression in pancreatic cancer cells. **M** HA130 (20 μM) decreases LPA concentration in conditioned media of pancreatic cancer cells. **N** The indirect co-culture model demonstrates that HA130 (10 μM) significantly impairs the repopulation ability of reporter cells. Dying cells were treated with DMSO, gemcitabine, HA130, or a combination of gemcitabine and HA130, and co-cultured with reporter cells for 48 h. All experiments were performed at least three times, and results are presented as mean ± standard deviation from three independent experiments. $*P < 0.05$, $**P < 0.01$, and $***P < 0.001$

However, a second downstream pathway involving iPLA2-LPC remains unexplored in tumor repopulation. Given that LPC was converted to via *ATX* [11], we selected LPA as the primary focus of this study among the upregulated lipids. Quantitative analysis revealed that while gemcitabine generally suppresses lipid metabolism in pancreatic cancer, it significantly elevates LPA concentrations in the conditioned medium (Fig. 2B and C). ELISA assays further confirmed a dose-dependent rise in LPA levels in conditioned media of pancreatic cancer cells treated with gemcitabine (Fig. 2D). Prior research has demonstrated that *LATS1/2* kinases inhibit *YAP1* activity by phosphorylating it, causing *pYAP1* sequestration in the cytoplasm through binding to 14-3-3 proteins [14]. LPA, however, inhibits *LATS1/2* through G12/13-coupled receptors, thus activating *YAP1* via dephosphorylation and nuclear translocation [12]. Based on these findings, we investigated whether similar mechanisms are involved in PDAC.

To explore the interaction between LPA and the Hippo signaling pathway in PDAC, we initially examined the expression of *YAP1* and *pYAP1* following LPA treatment. The results showed that LPA significantly reduced *YAP1* phosphorylation, promoted *YAP1* overexpression, and inhibited *ATX* expression (Fig. 2E and F). Subsequently, we assessed whether gemcitabine exerts effects comparable to those of LPA. Our findings indicated that gemcitabine similarly suppressed *YAP1* phosphorylation, enhanced *YAP1* expression, and reduced *ATX* protein expression (Fig. 2G and H). To investigate the effect of LPA and gemcitabine on *YAP1* localization, cytoplasmic and nuclear proteins were isolated separately and analyzed by Western blot. Upon stimulation with LPA or gemcitabine, an increase in *YAP1* nuclear localization was observed (Fig. 2I and J). Collectively, these results suggest that gemcitabine induces dying cells to release LPA in a dose-dependent manner, leading to diminished *YAP1* phosphorylation, increased *YAP1* nuclear translocation, and consequent inactivation of the Hippo pathway.

We also investigated the effects of LPA inhibition on the Hippo pathway. Western blot and RT-qPCR analyses revealed that HA130, an *ATX* activity inhibitor, significantly reduced *YAP1* expression while simultaneously increasing *ATX* protein expression (Fig. 2K and L). ELISA assay results confirmed that HA130 markedly decreased LPA concentrations in the conditioned medium of pancreatic cancer cells (Fig. 2M). These findings suggest that HA130 inhibits *YAP1* expression and enhances *ATX* protein level via negative feedback mechanisms.

We subsequently investigated the role of LPA in the repopulation of residual tumor cells driven by dying cells. Colony formation and transwell assays showed that LPA significantly enhanced the clonogenic and migratory capacities of pancreatic cancer cells, whereas HA130 significantly suppressed these effects (Fig. S1A-D). The CCK-8 assays revealed that reporter cells in the gemcitabine-treated group exhibited significantly enhanced proliferation compared to the control group, while no significant difference was observed between the HA130-treated and control groups (Fig. 2N). Notably, HA130 effectively reversed the pro-proliferative effects induced by dying cells following chemotherapy. These findings highlight that LPA inhibition serves as an effective strategy to suppress the proliferative potential of residual tumor cells.

In summary, our results demonstrate that gemcitabine induces a dose-dependent release of LPA from dying cells. This release leads to Hippo signaling inactivation, which subsequently enhances the colony formation, migration, and proliferative capacities of residual pancreatic cancer cells.

2.3 LPA promotes the repopulation of residual tumor cells through *YAP1*

To investigate the regulatory role of *YAP1* in PDAC, we initially analyzed transcriptome data from the TCGA database. Compared to adjacent tissues, *YAP1* mRNA levels were markedly elevated in PDAC (Fig. 3A). Kaplan-Meier survival analysis of TCGA-PDAC and GSE57495 cohorts revealed that patients with elevated *YAP1* expression exhibited significantly poorer overall survival (Fig. 3B). Additionally, *Pearson* correlation analysis revealed a negative correlation between *YAP1* and *ENPP2* (the gene encoding *ATX*, R = -0.15, p=0.044, Fig. 3C). Western blot and

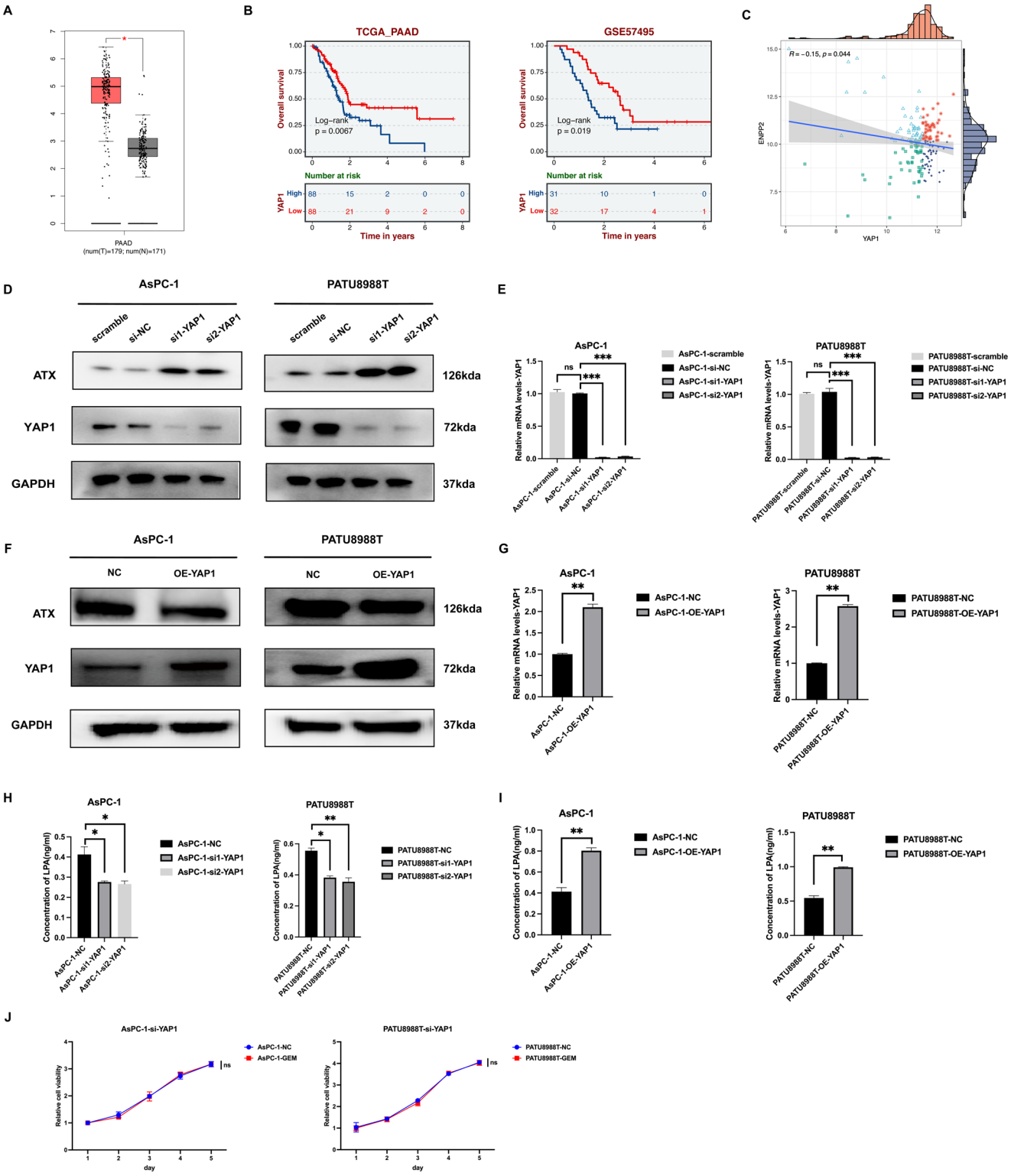
A
PAAD
(num(T)=179; num(N)=171)
B
TCGA_PAAD
Overall survival
Log−rank
p = 0.0067
Number at risk
High 88 15 2 0 0
Low 88 21 9 2 0
YAP1
Time in years
GSE57495
Log−rank
p = 0.019
High 31 10 1 0
Low 32 17 4 1
C
R = −0.15, p = 0.044
ENPP2
YAP1
D
AsPC-1
PATU8988T
scramble
si-NC
si1-YAP1
si2-YAP1
ATX
YAP1
GAPDH
126kda
72kda
37kda
E
AsPC-1
PATU8988T
Relative mRNA levels-YAP1
ns
AsPC-1-scramble
AsPC-1-si-NC
AsPC-1-si1-YAP1
AsPC-1-si2-YAP1
PATU8988T-scramble
PATU8988T-si-NC
PATU8988T-si1-YAP1
PATU8988T-si2-YAP1
F
AsPC-1
PATU8988T
NC
OE-YAP1
ATX
YAP1
GAPDH
126kda
72kda
37kda
G
AsPC-1
PATU8988T
Relative mRNA levels-YAP1
AsPC-1-NC
AsPC-1-OE-YAP1
PATU8988T-NC
PATU8988T-OE-YAP1
H
AsPC-1
PATU8988T
Concentration of LPA(ng/ml)
AsPC-1-NC
AsPC-1-si1-YAP1
AsPC-1-si2-YAP1
PATU8988T-NC
PATU8988T-si1-YAP1
PATU8988T-si2-YAP1
I
AsPC-1
PATU8988T
Concentration of LPA(ng/ml)
AsPC-1-NC
AsPC-1-OE-YAP1
PATU8988T-NC
PATU8988T-OE-YAP1
J
AsPC-1-si-YAP1
PATU8988T-si-YAP1
Relative cell viability
day
AsPC-1-NC
AsPC-1-GEM
PATU8988T-NC
PATU8988T-GEM
ns

Fig. 3 LPA promotes the repopulation of residual tumor cells through *YAP1*. **A** The differential *YAP1* expression between pancreatic cancer and adjacent tissues. **B** The comparison of overall survival between PDAC patients with high and low *YAP1* expression based on TCGA-PDAC and GSE57495 cohorts. **C** *Pearson* correlation analysis showing the negative relationship between *ENPP2* and *YAP1* expression. **D** Western blot was performed to detect the changes of *ATX* expression following *YAP1* knockdown in pancreatic cancer. **E** RT-qPCR validation of *YAP1* knockdown at the mRNA level. **F** Western blot was performed to detect the changes of *ATX* expression following *YAP1* overexpression in pancreatic cancer. Stable *YAP1*-overexpressing pancreatic cancer cell lines were generated using lentiviral transfection. **G** RT-qPCR validation of *YAP1* overexpression at the mRNA level. **H** ELISA results showing that *YAP1* knockdown reduces LPA concentration in conditioned media of pancreatic cancer cells. **I** ELISA results showing that *YAP1* overexpression increases LPA concentration in conditioned media of pancreatic cancer cells. **J** The indirect co-culture model illustrating that *YAP1* knockdown significantly inhibits the repopulation ability of pancreatic cancer reporter cells. Reporter cells with *YAP1* knockdown were co-cultured with dying cells treated with DMSO or gemcitabine for 48 h. All experiments were performed in biological triplicates, and data are presented as mean ± standard deviation from three independent experiments. Kaplan-Meier analysis and log-rank test were performed to evaluate overall survival differences between distinct subgroups. Statistical significance was determined as $*P < 0.05$, $**P < 0.01$, and $***P < 0.001$

RT-qPCR results showed that *YAP1* knockdown led to a pronounced increase in *ATX* expression (Fig. 3D and E). We further established stable pancreatic cancer cell lines with *YAP1* overexpression via lentiviral transfection (Fig. 3F and G). Western blot results revealed that *YAP1* overexpression significantly suppressed *ATX* expression.

ELISA assays were performed to explore whether *YAP1* regulates the levels of LPA. The results showed that *YAP1* knockdown significantly reduced LPA concentrations in the conditioned medium, whereas *YAP1* overexpression resulted in increased LPA levels (Fig. 3H and I). These findings revealed that *YAP1* knockdown inhibits *ATX* activity, thereby suppressing LPA production. Conversely, *YAP1* overexpression enhanced LPA synthesis and release, with LPA exerting a negative feedback effect on *ATX* expression. We also conducted transwell and colony formation assays to evaluate the oncogenic function of *YAP1*. As expected, *YAP1* overexpression promoted both colony formation and cell migration of pancreatic cancer (Fig. S1E-H). Finally, we investigated the role of *YAP1* in tumor repopulation through indirect co-culture, and the results showed that after knockdown of *YAP1*, the difference in proliferation rate between gemcitabine-treated group and control group was nearly negligible (Fig. 3J). In summary, these findings suggest that chemotherapy-induced dying cells release LPA to facilitate *YAP1* nuclear translocation. This, in turn, further amplifies LPA release, establishing a positive feedback loop between LPA and *YAP1*.

2.4 HA130 enhances gemcitabine-induced apoptosis and DNA damage

Gemcitabine primarily functions by incorporating into DNA strands, thereby inhibiting DNA replication and inducing cell death [15]. Therefore, Gene set enrichment analysis (GSEA) was performed to further examine the effect of *YAP1* on DNA replication-associated processes. The results indicated that *YAP1* notably modulates DNA repair, G2M checkpoint, DNA damage checkpoint, and cell cycle DNA replication (Fig. 4A). These findings suggest that the combination of gemcitabine and HA130 could serve as a promising therapeutic strategy.

Based on the Synergyfinder database (https://synergyfinder.org/#!/dashboard), we evaluated potential synergy or antagonism between the two drug combinations. The CCK-8 assays were performed to measure absorbance per well, allowing us to calculate dose-response matrices for each drug concentration and corresponding cell viability [16]. A synergy score below 0 indicates drug antagonism, a score between 0 and 10 suggests additive effects, and a score above 10 indicates synergy between the drug combinations. The results revealed synergy scores of 21.83 and 13.16 for the HA130 and gemcitabine combination in AsPC-1 (Fig. 4B and C) and PATU8988T (Fig. 4D and E), respectively, demonstrating a pronounced synergistic effect between the two drugs.

To explore the synergistic induction of apoptosis in pancreatic cancer by combination therapy, we assessed the effects of inhibiting LPA-*YAP1* signaling using flow cytometry. Our study revealed that the combination of gemcitabine with HA130 or si-*YAP1* significantly increased the proportion of apoptotic cells compared to monotherapy groups (Fig. 4F and G). Additionally, Western blot analysis confirmed that combination treatment markedly enhanced the capacity of gemcitabine to induce DNA damage in pancreatic cancer (Fig. 4H). These findings suggest that targeting the LPA-*YAP1* signaling may be an effective strategy to improve chemotherapy efficacy in pancreatic cancer.

2.5 Single-cell sequencing reveals *YAP1* may regulate chemokines and cholesterol

Single-cell RNA sequencing analysis (scRNA-seq) of the GSE212966 dataset was employed to investigate the impact of *YAP1* on the tumor microenvironment (TME) of pancreatic cancer. The quality control process adhered strictly to the standard protocol outlined in the Materials and Methods section (Fig. S2A-J). Using the "SingleR" package, we identified 13 cell types, including fibroblasts, macrophages, endothelial cells, epithelial cells (tumor cells), NK cells, T cells, monocytes, smooth muscle cells, neurons, and

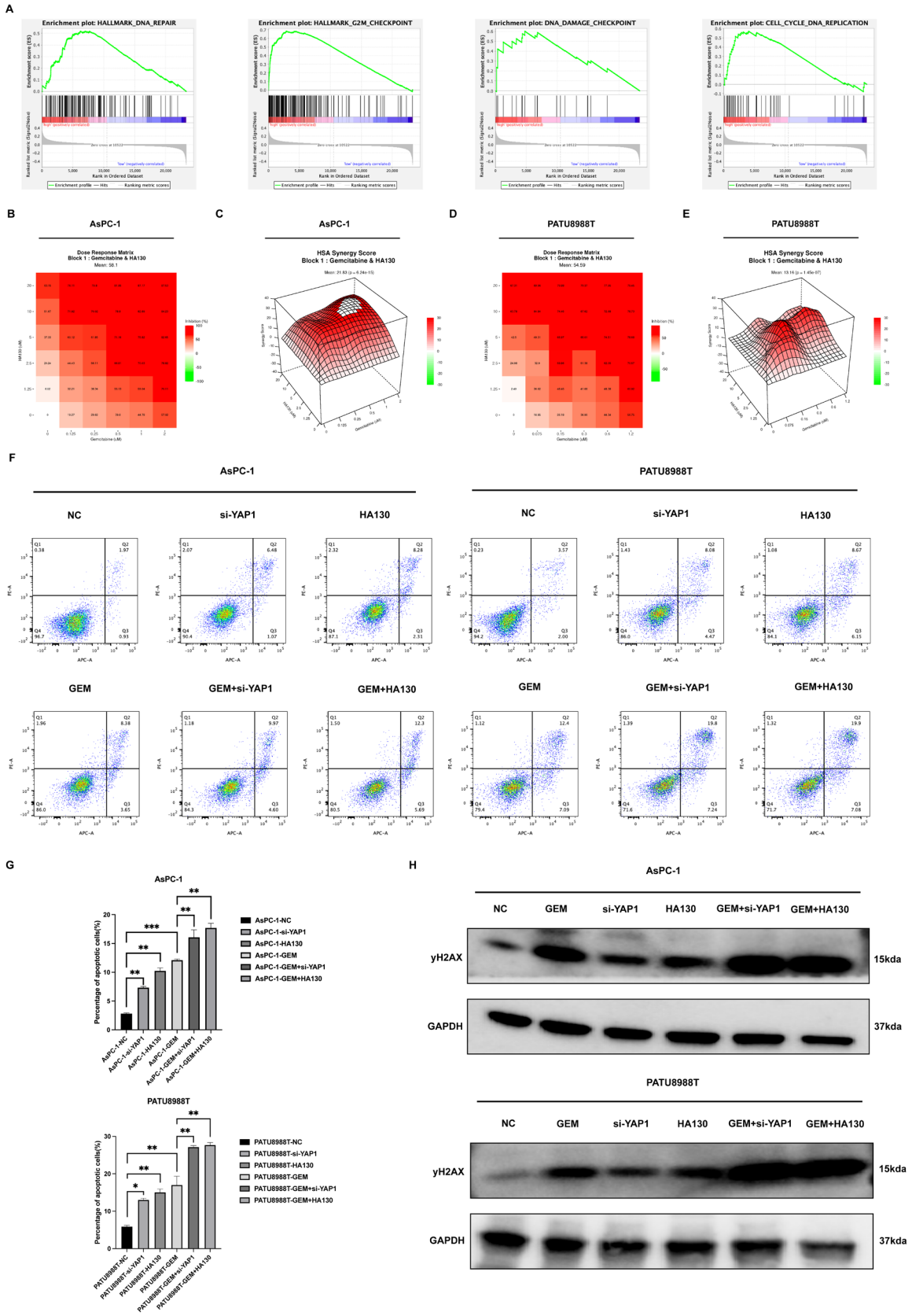
A
Enrichment plot: HALLMARK_DNA_REPAIR
Enrichment plot: HALLMARK_G2M_CHECKPOINT
Enrichment plot: DNA_DAMAGE_CHECKPOINT
Enrichment plot: CELL_CYCLE_DNA_REPLICATION
B
AsPC-1
Dose Response Matrix
Block 1 : Gemcitabine & HA130
C
AsPC-1
HSA Synergy Score
Block 1 : Gemcitabine & HA130
D
PATU8988T
Dose Response Matrix
Block 1 : Gemcitabine & HA130
E
PATU8988T
HSA Synergy Score
Block 1 : Gemcitabine & HA130
F
AsPC-1
PATU8988T
NC
si-YAP1
HA130
GEM
GEM+si-YAP1
GEM+HA130
G
AsPC-1
Percentage of apoptotic cells(%)
AsPC-1-NC
AsPC-1-si-YAP1
AsPC-1-HA130
AsPC-1-GEM
AsPC-1-GEM+si-YAP1
AsPC-1-GEM+HA130
PATU8988T
PATU8988T-NC
PATU8988T-si-YAP1
PATU8988T-HA130
PATU8988T-GEM
PATU8988T-GEM+si-YAP1
PATU8988T-GEM+HA130
H
AsPC-1
NC
GEM
si-YAP1
HA130
GEM+si-YAP1
GEM+HA130
yH2AX
GAPDH
15kda
37kda
PATU8988T

Fig. 4 HA130 enhances gemcitabine-induced apoptosis and DNA damage. **A** Gene set enrichment analysis (GSEA) showing that *YAP1* activation enhances pathways related to DNA repair, G2/M checkpoint, DNA damage checkpoint, and DNA replication in pancreatic cancer. **B** Highest single agent (HSA) synergy score matrix assessing the synergistic effect of gemcitabine and HA130 in AsPC-1 cells. The X-axis represents gemcitabine concentrations, the Y-axis represents HA130 concentrations, and synergy scores are displayed as matrix values. **C** Dose-effect matrix for the combination of gemcitabine and HA130 in AsPC-1 cells, where gemcitabine concentration is on the X-axis, HA130 concentration is on the Y-axis, and inhibition rates are represented as matrix values. **D** HSA synergy score matrix evaluating the synergistic effect of gemcitabine combined with HA130 in PATU8988T cells. The X-axis represents gemcitabine concentrations, the Y-axis represents HA130 concentrations, and synergy scores are shown as matrix values. **E** Dose-effect matrix for gemcitabine and HA130 combination in PATU8988T cells, with gemcitabine concentration on the X-axis, HA130 concentration on the Y-axis, and inhibition rates shown as matrix values. **F** Combined treatment of gemcitabine with si-*YAP1* or HA130 enhances apoptosis in pancreatic cancer cells. Cells in quadrants q2 and q4 are identified as apoptotic cells. **G** The differences of apoptosis ratio in different treatment groups. **H** The combination of gemcitabine with si-*YAP1* or HA130 promotes DNA damage in pancreatic cancer cells, as assessed by western blot analysis of *γH2A.X* with *GAPDH* as the internal control. All experiments were performed in triplicate, and data are presented as mean ± standard deviation from three independent experiments. Statistical significance was determined as $*P < 0.05$, $**P < 0.01$, and $***P < 0.001$

other cell types (Fig. 5A). The single sample GSEA results indicated significant variations in the activity of Hippo signaling across different cell types (Fig. 5B). Consistent with expectations, the median level of Hippo signaling in pancreatic cancer is lower than that observed in adjacent tissues (Fig. 5C). Additionally, *YAP1* expression level is significantly higher in pancreatic cancer compared to *ENPP2* (Fig. 5D and E). The uniform manifold approximation and projection (UMAP) distribution plot indicated that cell types with high *YAP1* expression generally did not express *ENPP2*, and vice versa (Fig. 5F). To gain a deeper understanding of Hippo pathway-related genes, we also depicted their UMAP distribution (Fig. S3) and analyzed the expression differences between adjacent tissues and pancreatic cancer (Fig. S4).

We further examined the proportion of epithelial cells (tumor cells) expressing high and low levels of *YAP1*. The result indicated a higher proportion of epithelial cells with elevated *YAP1* levels in pancreatic cancer (Fig. 5G). Differential gene analysis was conducted on epithelial cells based on *YAP1* expression levels (Table s1), followed by KEGG and GO enrichment analyses. These analyses revealed that *YAP1* primarily regulates pathways involved in chemokine signaling, TNF signaling, and the extracellular matrix (Fig. 5H). Several studies have reported that interleukin 6 (*IL6*) and interleukin 8 (*IL8*) are regulated by different signaling axes mediated by *YAP1*, which enhance the malignancy of various tumors [17, 18]. *Pearson* correlation analysis of the TCGA-PDAC cohort revealed that *YAP1* also demonstrated positive correlations with *IL8* and *IL6*, with correlation coefficients of 0.61 and 0.23, respectively (Fig. S2K and L). RT-qPCR results demonstrated that *YAP1* knockdown significantly inhibited *IL6* and *IL8* expression, whereas *YAP1* overexpression notably promoted their upregulation (Fig. 5I and J). ELISA assays further confirmed the positive regulatory effect of *YAP1* on *IL6* and *IL8* (Fig. 5K and L). These findings suggest that gemcitabine-induced overexpression of *YAP1* may elevate the levels of several critical chemokines, thereby fostering an inflammatory TME in pancreatic cancer.

The "AUCell" and "UCell" algorithms were used to perform GSEA at the single-cell level. The results indicated that *YAP1* significantly enhanced cholesterol homeostasis (Fig. 5M), which was corroborated by GSEA conducted on the TCGA-PDAC cohort (Fig. 5N). Numerous studies have emphasized the role of *YAP1* in cholesterol synthesis across various types of tumors [19–21]. The accumulation of cholesterol and oxysterols inactivates the sterol regulatory element-binding protein-2 (*SREBP2*) pathway by promoting the retention of the *SREBP* Cleavage-Activating Protein-*SREBP2* complex in the endoplasmic reticulum, which in turn downregulates cholesterol biosynthesis and uptake [19]. RT-qPCR results demonstrated that *YAP1* overexpression significantly upregulated *SREBP2* expression, while *YAP1* knockdown resulted in a decrease in *SREBP2* levels (Fig. 5O). Given that cholesterol metabolism serves as a potential target for modulating cancer-related processes [20, 21], these findings imply that interventions in the Hippo signaling pathway may offer an effective strategy to improve the TME following chemotherapy in pancreatic cancer.

3 Discussion

PDAC is a highly malignant tumor of the digestive system, projected to become the second leading cause of cancer-related death in the United States by 2030 [22]. Patients with pancreatic cancer are often diagnosed at an advanced stage, resulting in a grim prognosis. Gemcitabine is widely used as the first-line chemotherapy for PDAC [23, 24]. However, its response rate remains remarkably low, with most patients rapidly developing resistance to the treatment. Emerging evidence suggests that metabolic reprogramming constitutes a novel mechanism of chemotherapy resistance [25]. Lipid metabolism reprogramming has been recognized as a hallmark of malignancies. Tumor-associated alterations in lipid metabolism primarily encompass increased lipogenesis, enhanced lipid uptake from the extracellular microenvironment, and elevated lipid storage and mobilization within intracellular lipid droplets [26]. Tumor repopulation, characterized by the accelerated growth of residual tumor cells

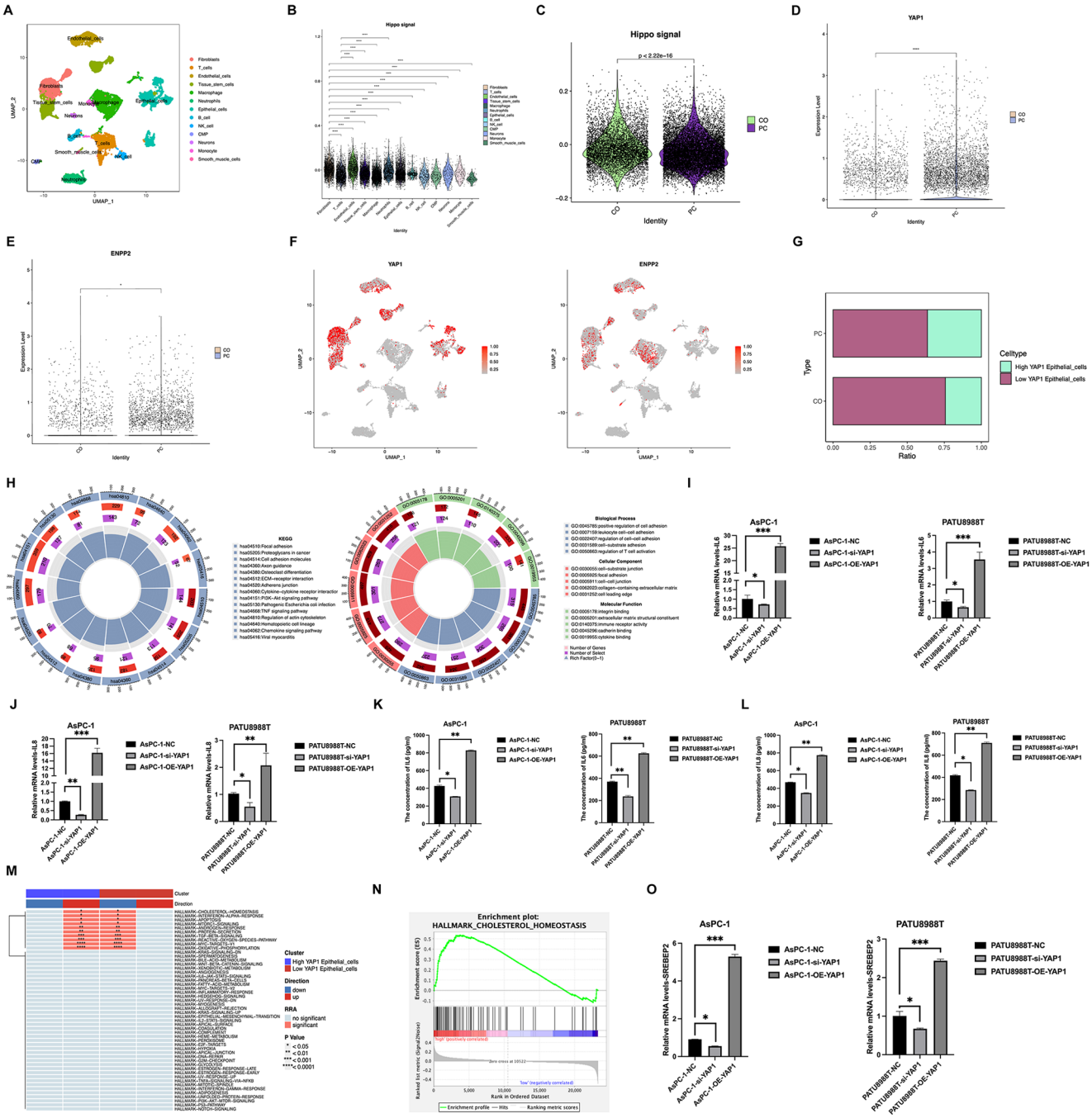

Fig. 5 Single-cell sequencing reveals *YAP1* may regulate multiple chemokines. **A** The UMAP distribution of different cell types annotated using the "SingleR" package. **B** The activity of Hippo signaling varies across different cell types. The *wilcoxon* test was used to compare differences in Hippo signaling activity among different cell types at the single-cell level. **C** The violin Plot showing differences in Hippo signaling between adjacent tissues (CO) and pancreatic cancer (PC). **D**, **E** The expression levels of *YAP1* and *ENPP2* across different subgroups. **F** The UMAP distribution diagram showing the expression of *ENPP2* and *YAP1* across various cell types. **G** The proportion of epidermal cells expressing high versus low levels of *YAP1* across different samples. **H** Kyoto Encyclopedia of Genes and Genomes (KEGG) and Gene Ontology (GO) functional enrichment analysis of differentially expressed genes (DEGs) between epidermal cells with high versus low *YAP1* expression. **I** RT-qPCR results indicate that *YAP1* knockdown inhibits *IL6* mRNA expression, while *YAP1* overexpression promotes it. **J** RT-qPCR results show that *YAP1* knockdown reduces *IL8* mRNA expression, while *YAP1* overexpression enhances it. **K**, **L** The ELISA assays confirm that *YAP1* positively regulates *IL6* and *IL8* levels. **M** Pathway differences identified between epidermal cells with high- and low-*YAP1* expression by single-sample gene set enrichment analysis. **N** GSEA analysis based on the TCGA-PDAC cohort confirms that *YAP1* promotes cholesterol homeostasis. **O** RT-qPCR results showing that *YAP1* knockdown decreases *SREBP2* mRNA expression, while *YAP1* overexpression increases its expression. All experiments were performed in triplicate, and data are presented as mean ± standard deviation from three independent experiments. Statistical significance was determined as $*P < 0.05$, $**P < 0.01$, $***P < 0.001$ and $****P < 0.0001$

following chemoradiotherapy, also contributes to resistance against these treatments [27, 28]. Both lipid metabolism and tumor repopulation are critical contributors in chemotherapy failure; however, the underlying correlations and mechanisms remain to be fully elucidated. In this study, direct and indirect co-culture models were used to mimic the in *vivo* environment, demonstrating that gemcitabine-induced dying cells can promote the regeneration of residual pancreatic cancer cells through the release of LPA.

Ample evidence indicates that abnormal lipid metabolism-encompassing membrane formation, lipid synthesis and degradation, and lipid-driven signaling plays a crucial role in various cancers [29]. Fatty acid synthase (*FASN*), a key lipogenic enzyme in de novo fatty acid synthesis, is involved in the regulation of plasma membrane structure and palmitoylation of proteins post-translationally [30]. In pancreatic cancer, *FASN* overexpression is associated with adverse reactions to gemcitabine, primarily due to the upregulation of pyruvate kinase M2 [31]. Transcriptionally, *FASN* is primarily regulated by the *SREBP* family, which is influenced by *PI3K/AKT* and *MEK/ERK* pathway [32]. Previous studies have highlighted that lipid not only plays a crucial role in the formation of biological membranes and energy metabolism, but also functions as second messengers regulating tumor progression [29, 33]. Specifically, phospholipases generate several second messengers, such as LPA and AA, which activate multiple carcinogenic pathways [34, 35]. Emerging evidence underscores the physiological role of LPA in regulating tumor progression, angiogenesis, and metastasis [36]. LPA is a bioactive phospholipid that engages with at least six receptors, namely LPAR1-6, each coupled to a specific G-protein [37]. LPA is produced by hydrolysis of LPC mediated by *ATX* (LPA synthetase). Our previous research has confirmed the critical role of *ATX* in driving the malignancy of pancreatic cancer [11]. It has been reported that *ATX* also serves as a biomarker for early diagnosis [38]. Consequently, we focused on the impact of gemcitabine on lipid metabolism, particularly investigating whether dysregulated LPA metabolism following chemotherapy contributes to drug resistance and repopulation in pancreatic cancer. As expected, while gemcitabine generally suppresses lipid metabolism in pancreatic cancer cells, it aberrantly induces a significant increase in LPA levels.

Hippo is a crucial anti-cancer pathway in *vivo*, wherein mammalian Sterile 20-like kinase 1/2 (*MST1/2*) and *LATS1/2* are activated through various mechanisms [39]. By phosphorylating the transcription factors *YAP1*/*TAZ*, *LATS1/2* facilitates the binding of *YAP1* to 14-3-3 proteins in the cytoplasm, thereby exerting a cancer-inhibiting effect. When *LATS1/2* activity decreases, *YAP1/TAZ* translocates to the nucleus in an unphosphorylated state, promoting tumor proliferation, invasion, and the maintenance of stem-like properties [40]. Our research group was the first to report that *TAZ*, an effector of the Hippo pathway, is highly expressed in pancreatic cancer and facilitates metastasis by enhancing epithelial-mesenchymal transition [41]. Based on existing evidence and mass spectrometry analysis, our study proposes the hypothesis that gemcitabine induces the release of LPA from dying pancreatic cancer cells, which subsequently regulates the nuclear translocation of *YAP1* in residual tumor cells, thereby promoting tumor repopulation.

Mechanistic studies have revealed that both gemcitabine and LPA inhibit *YAP1* phosphorylation in a dose-dependent manner, ultimately leading to the inactivation of the Hippo pathway. In the context of pancreatic cancer, we observed a negative correlation between *ATX* and *YAP1*. Both gemcitabine and LPA also enhanced *YAP1* translocation and reduced *ATX* protein expression through a complex feedback mechanism. Additionally, *YAP1* overexpression exhibited effects similar to those induced by gemcitabine and LPA. While several studies have reported that various factors can activate *YAP1* to enhance the malignancy of solid tumors [18, 42], the relationship between *YAP1* and post-chemotherapy repopulation in pancreatic cancer remains unclear. Our findings suggest the presence of an LPA-*YAP1* positive feedback loop in the TME following chemotherapy (Fig. 6). The results from the indirect co-culture model further confirmed that *YAP1* suppression in reporter cells abrogated the pro-proliferative effect of dying cells. Classical molecular biology experiments suggest that targeting the LPA-*YAP1* axis may serve as a potential strategy to enhance chemotherapy efficacy.

The upregulation of the *ATX*-LPA signaling in tumor cells can effectively induce lymphocyte entry into secondary lymphoid organs, indicating the complex regulatory role of LPA in the TME [43]. Therefore, the potential impact of the LPA-*YAP1* signal on TME warrants further exploration. The results of single-cell sequencing analysis revealed that *YAP1* might regulate the levels of various chemokines and cholesterol, highlighting a significant role of *YAP1* in metabolic reprogramming. Furthermore, GO analysis suggests that *YAP1* may be involved in T cell activation and immune receptor activity, implying that targeting LPA-*YAP1* signaling could enhance the potential for immunotherapy response in pancreatic cancer patients.

We humbly acknowledge the limitations of our study. Primarily, our research focused solely on in *vitro* mechanistic studies and lacked in *vivo* validation. Currently, a stable mouse model for chemotherapy-induced repopulation has not yet been established. Furthermore, additional investigation is necessary to optimize the dosage and administration intervals of gemcitabine in *vivo*.

Altogether, we demonstrated that gemcitabine induces the release of LPA from dying pancreatic cancer cells,

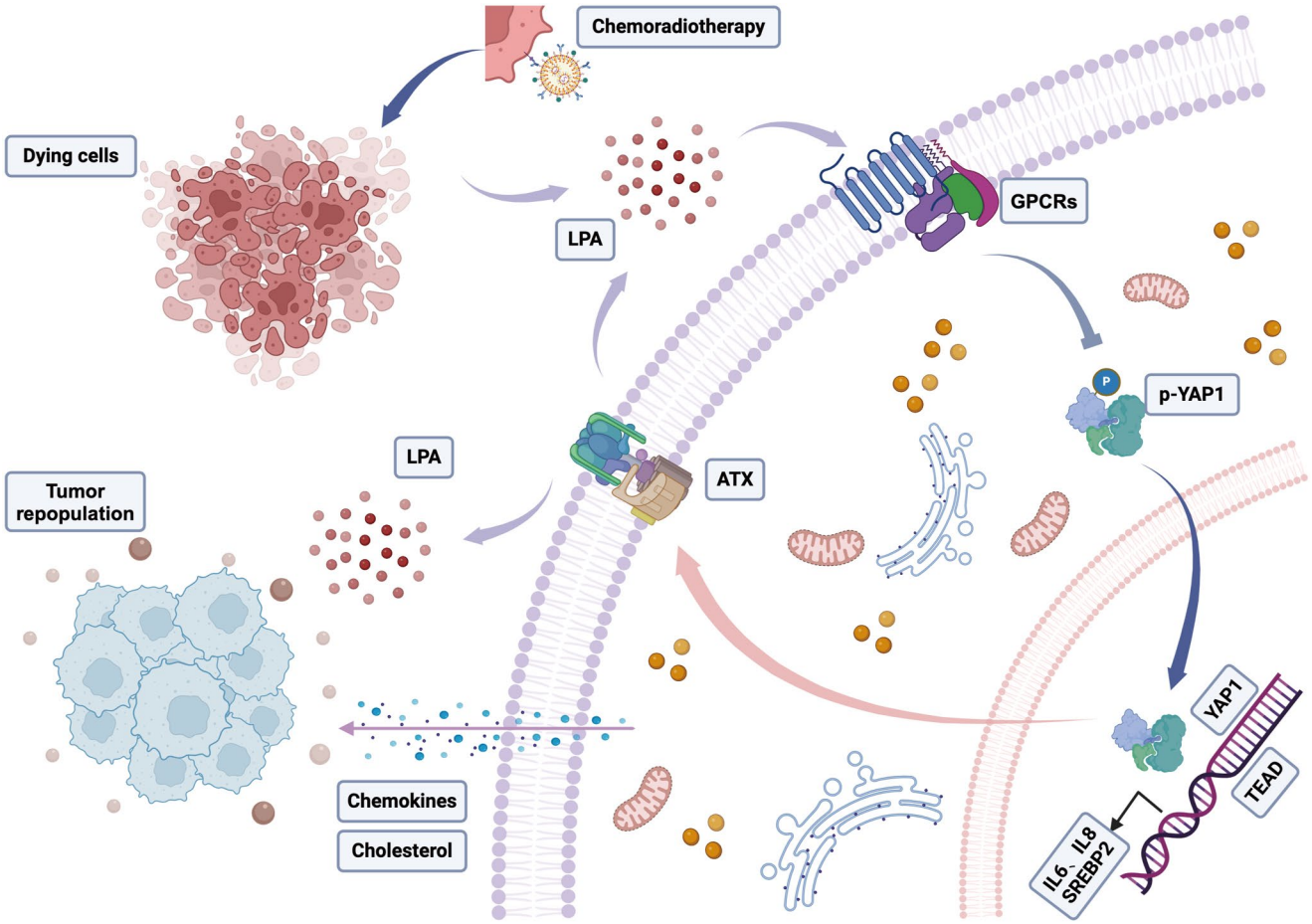

Fig. 6 Mechanisms of post-chemotherapy repopulation in pancreatic cancer. GPCRs, G-protein-coupled receptors; *TEAD*, transcriptional enhanced associate domain

which in turn inhibits *YAP1* phosphorylation and promotes its nuclear translocation. On the one hand, *YAP1* overexpression facilitates the release of LPA, thereby forming a positive feedback loop between LPA and *YAP1*. On the other hand, *YAP1* elevates chemokines and cholesterol levels, fostering a TME that supports pancreatic cancer survival. These mechanisms underscore the potential of targeting the LPA-*YAP1* signaling axis to overcome chemoresistance and reduce recurrence in pancreatic cancer.

4 Methods

4.1 Materials and reagents

The components and reagents used in this study were sourced from the following companies: RPMI 1640 culture medium (Roswell Park Memorial Institute, Gbico, USA), Penicillin-Streptomycin solution (100 ×) (Hangzhou Jino Company), 10 × PBS (Biyuntian Company), DMSO and Polybrene (Sigma), fetal bovine serum (FBS) (Hyclone, USA), 0.25% trypsin-EDTA, Lipofectamine 3000, and puromycin (Gibco), and D-luciferin substrate (Promega).

4.2 Cell culture

Human pancreatic carcinoma cell lines, PATU8988T and AsPc-1, were obtained from the American Type Culture Collection (Manassas, VA, USA). These cells were cultured at 37 °C in a humidified incubator with 5% CO_2, using RPMI 1640 medium supplemented with 10% FBS. Short tandem repeat analysis was performed to verify the identities of the cell lines, all of which were confirmed to be free of mycoplasma contamination.

4.3 Tumor repopulation cell model

Pancreatic cancer cells were treated with 1~5 μM gemcitabine (Cat# HY-17026, MedChem Express, NJ, USA) for 48 to 72 h, washed twice with 1 × PBS, and the supernatant was discarded. The medium was then replaced with 2% serum, and the cells were incubated for an additional 24 h.

The adherent dying cells were collected and referred to as the experimental group (gemcitabine treatment). The term "dying cell" broadly refers to cells undergoing programmed cell death, which can be characterized by morphological changes, DNA fragmentation, activation of caspase family proteases, and decreased metabolic activity [44]. Classical morphological features indicative of impending cell death, such as cell contraction, detachment from neighboring cells, and altered membrane integrity, can be observed under the microscope. The control group consisted of dying cells treated with DMSO for 48 to 72 h, with subsequent treatment procedures identical to those of the experimental group.

In the direct co-culture model, 1×10^5 dying cells were evenly seeded in 24-well plates. After attachment, 1000 GFP-labeled pancreatic cancer cells (reporter cells) were uniformly seeded on top. The medium containing 2% serum was replaced every 48 h. Images were captured every 48 h using a fluorescence microscope to monitor the proliferation activity of the reporter cells.

In the indirect co-culture model, 1×10^5 normal pancreatic cancer cells were uniformly seeded in 24-well plates. Once the cells adhered, transwell inserts (Cat# 725122, NEST, Wuxi, China) containing 3×10^5 dying cells with a 0.4 μm pore size were placed in each well, ensuring that the lower part of the transwell inserts was submerged in medium containing 2% serum. After 48 h, the adherent pancreatic cells (reporter cells) in the lower chamber were collected, and their proliferation activity was assessed using a CCK-8 assay (Cat# C0037, Beyotime, Shanghai, China).

4.4 Identification of differential lipids using mass spectrometry analysis

Lipidomic profiling of supernatants from pancreatic cancer cells was performed using liquid chromatography-tandem mass spectrometry (LC-MS/MS) in both positive and negative ion modes to detect a range of lipid molecules. The analysis was conducted in the following steps: (1) The samples underwent lipid extraction using the Bligh and Dyer method, ensuring integrity of lipid components. The extracted lipids were dried and dissolved in a dichloromethane/methanol mixture for subsequent analysis. Reverse-phase liquid chromatography was used for chromatographic separation, with an optimized gradient elution program to achieve effective categorization of lipid classes. (2) Full scan and data-dependent acquisition modes were utilized to obtain detailed lipid molecular and fragment information. The analysis system comprised ultra-performance liquid chromatography (UPLC, ExionLC™ AD and tandem mass spectrometry (MS/MS, QTRAP® 6500+ (https://sciex.com.cn/). Raw mass spectrometry data were preprocessed using mass spectrometry-data independent analysis software, including peak extraction, alignment, and noise reduction. (3) Quantification results were normalized using methods such as total ion intensity normalization and principal component analysis. Lipid molecules were subsequently identified and annotated based on the human metabolome database (https://hmdb.ca/). All detection and analyses were provided by Wuhan Metware Biotechnology Co., Ltd.

4.5 Flow cytometry for apoptosis detection

Pancreatic cancer cells (1×10^5 cells/mL) were allowed to grow for 24 h in a 6-well plate containing RPMI 1640 medium supplemented with 10% FBS. Subsequently, the cells were treated with gemcitabine (1 μM). After 48 h, the cells were harvested and washed with cold PBS buffer. They were then resuspended in a binding buffer and stained in the dark with 5 μL of Annexin V-FITC and 5 μL of propidium iodide (Cat# C1383S, Beyotime, Shanghai, China) at 4 °C for 30 min. The stained cells were washed three times with binding buffer to remove excess dye and then resuspended in 500 μL of binding buffer. Untreated cells served as negative controls. The percentage of apoptotic cells was analyzed within 1 h using flow cytometry (BD, FACSCalibur, USA).

4.6 CCK-8 assay for the detection of proliferation

Cell viability was assessed using the CCK-8 following the manufacturer's instructions. Cells were seeded in a 96-well microplate at a density of 3×10^3 cells per well in 100 μL of culture medium. Every 24 h, 10 μL of CCK-8 reagent was added to each well, followed by a 1-hour incubation. The absorbance was measured at 450 nm using a microplate reader (Bio-Rad, Hercules, CA, USA).

4.7 Transwell migration assay

Complete medium (1 mL) was added to the lower chamber of the transwell invasion system. Subsequently, pancreatic cancer cells were resuspended in serum-free medium and seeded into the upper chamber at a density of 5×10^4 cells per well. After 24 h of incubation, we quantitatively assessed the number of cancer cells that traversed the membrane using ImageJ software. The images were converted to grayscale, and threshold adjustments were made to separate the cells from the background. The analyze particle function was used to calculate the number of migrated cells. We repeated the experiments multiple times to reduce variability and calculated the average.

4.8 Colony formation assay

Reporter cells were resuspended in RPMI 1640 medium containing 10% FBS and incubated at 37 °C in a 5% CO_2 environment for 7 to 14 days. A total of 3000 cells were seeded per well to facilitate colony formation. After incubation, the plates were washed with cold PBS, and the colonies were fixed with 4% paraformaldehyde (Cat# P0099-3 L, Beyotime, Shanghai, China) at room temperature. The fixed colonies were then stained with 1% crystal violet for 30 min at room temperature. Colonies containing more than 100 cells were counted using ImageJ software.

4.9 Lentivirus transduction

1×10^6 pancreatic cancer cells were inoculated in the six-well plate, and the medium was discarded after 24 h when the cell fusion reached about 80%. Next, 1 mL of viral culture medium was mixed with 1 mL of fresh culture medium containing Polybrene (final concentration 1:1000) and added to the cells for continued cultivation. After 24 h of infection, GFP expression in the tumor cells was assessed under a fluorescence microscope. Cells exhibiting uniform GFP brightness were collected and transferred to 10 cm culture dishes for continued cultivation.

To generate stable cells expressing the exogenous gene GFP-Luc, puromycin (1 μg/mL) was added 24 h post-infection for selection. The culture medium was replaced every 3 days, with fresh puromycin added for selection over 2 weeks. This process yielded double-labeled cells, namely AsPC-1/GFP-Luc and PATU8988T/GFP-Luc. The expression of GFP in the cells was accessed and photographed under a fluorescence microscope. The labeled cells were expanded, and corresponding cell lines were stored for future use.

4.10 Western blot

Pancreatic cells were collected by centrifugation and washed twice with cold PBS. The cell pellets were suspended in 100 μL of cold RIPA lysis buffer and incubated on ice for 30 min, with vortexing every 10 min. Cytoplasmic and nuclear protein was separated and extracted using the NE-PER™ nuclear and cytoplasmic extract reagent kit (Cat# 78833, Thermo Fisher, MA, USA). The samples were then centrifuged at 15,000 g for 30 min. Immunoblot analysis was performed using 10 μg of sample proteins on a 12% SDS-PAGE gel. Electrophoresis was conducted at 120 V for 60 min to separate the proteins, followed by transfer to a PVDF membrane in cold transfer buffer using a wet transfer system at 300 mA for 90 min.

The PVDF membrane was blocked for 1 h and then incubated with primary antibodies (diluted 1:1000) overnight at 4 °C. After washing, the membrane was incubated with secondary antibodies (diluted 1:4000) at room temperature for 1.5 h. Protein bands were visualized using an ECL protein blot detection system (Tanon 4200), and band intensities were analyzed using Quantity One software. The antibodies against *YAP1* (Cat# 4912 S) and *pYAP1* (Ser 397, Cat# 13619T) were obtained from Cell Signaling Technology, Inc. (Boston, USA). The antibody against *ATX* (Cat# abs116120) was purchased from Absin Bioscience Inc. (Shanghai, China). The antibodies against *Lamin B* (Cat# ab16048), *γH2A.X* (Ser 139, Cat# ab26350) and *GAPDH* (Cat# ab263962) were sourced from Abcam, Inc. (Cambridge, USA). Secondary antibodies against rabbit (Cat# BA1060) or mouse (Cat# BM2002) were purchased from Boster Biotechnology (Wuhan, China).

4.11 Real-time quantitative reverse transcription polymerase chain reaction

According to the manufacturer's instructions, cDNA was generated using the RevertAid First Strand cDNA Synthesis Kit (Thermo Scientific). Reverse transcription quantitative polymerase chain reaction (RT-qPCR) was performed using PowerUp SYBR Green Master Mix (Thermo Fisher). β-actin was used as the internal control. The primer sequences are listed in Table s2.

4.12 ELISA

Following the manufacturer's instructions, the levels of LPA in the conditioned medium were assessed using an ELISA kit from Bioo Scientific, Inc. (Cat# EH11121M). Additionally, the concentrations of *IL6* and *IL8* in the conditioned medium were determined using ELISA kits obtained from eBioscience Inc. (Cat# EH2IL6) and BioLegend Inc. (Cat# 431504), respectively.

4.13 Single-cell sequencing analysis and RNA-sequencing analysis

The pancreatic cancer scRNA-seq data, GSE212966 [45], was downloaded from the Gene Expression Omnibus database (GEO, https://www.ncbi.nlm.nih.gov/geo/). A total of 44 Hippo pathway-related genes were curated from the MSigDB database (https://www.gsea-msigdb.org/gsea/msigdb/human/search.jsp). The detailed processing of the scRNA-seq data was conducted as follows: (1) The scRNA-seq data was preprocessed using the "Seurat" package. The "PercentageFeatureSet" function was employed to determine the proportion of mitochondrial genes, followed by

correlation analysis to investigate the relationship between sequencing depth and the proportion of mitochondrial genes or total intracellular sequences. (2) Each gene was required to be expressed in at least 3 cells. (3) Cells were included if they expressed between 300 and 5000 genes, had mitochondrial content below 20%, and the unique molecular identifier (UMI) count exceeding 1000. (4) After filtering, the dataset was normalized using the "LogNormalize" method to ensure consistency in gene expression values.

We analyzed a total of 38,981 cells from six scRNA-seq samples, of which 34,208 cells were retained after quality control (Table s3). As shown in Fig. S2A and B, there is a strong correlation between UMI count and mRNA ($r=0.85$). However, no significant correlation was observed between mRNA counts and mitochondrial or ribosomal gene content. The top 2000 highly variable genes were identified for subsequent dimensionality reduction analysis (Fig. S2C). We used the principal component analysis (PCA) to estimate available dimensions and depicted the raw distribution of different samples. The result showed no substantial differences among all cells (Fig. S2D and E). The top 30 most unique principal components were selected for further investigation (Fig. S1F). After removing batch effects, we visualized the combined distribution of the CO (adjacent tissues) and PC (pancreatic cancer) samples (Fig. S2G and H). The gene expression patterns of the top 15 principal components were further examined (Fig. S1I). Guided by the clustering tree, we set the resolution parameter to 1, resulting in the identification of 34 distinct clusters. (Fig. S1J).

The RNA-sequencing expression data and clinical features of PDAC were downloaded from the Cancer Genome Atlas database (TCGA, https://portal.gdc.cancer.gov/). The RNA-sequencing expression profiles in the GSE57495 dataset were also retrieved from the GEO database [46]. The detailed processing of the microarray data was as follows: (1) Gene symbols were obtained by converting probe IDs. (2) Probes that corresponded to multiple genes were removed. (3) When multiple probes corresponded to a single gene, the average value of these probes was considered as the gene expression level.

4.14 Statistical analysis

Statistical analysis was conducted using *R* (version 4.2.3) and GraphPad Prism 7 (CA, USA). The *wilcoxon* test was used to compare differences in Hippo signaling activity among various cell types at the single-cell level. *Pearson* correlation analysis was employed to assess the linear relationships between different genes. Kaplan-Meier analysis and log-rank test were performed to evaluate survival differences between distinct subgroups. Student's *t*-test and analysis of variance (*ANOVA*) were employed to compare quantitative data between groups. All experiments were performed using representative data in triplicate and independently repeated at least three times. Results are presented as the mean ± standard deviation from three or more experimental replicates. $P<0.05$ was considered statistically significant.

Supplementary Information The online version contains supplementary material available at https://doi.org/10.1007/s13402-025-01038-9.

Acknowledgements We are grateful for the support of lipidomics analysis provided by Wuhan Metware Biotechnology Co., Ltd.

Author contributions LY, DJ and LS contributed equally to this work. LY: design of the work and the implementation of the experiment. DJ: implementation of the experiment and write the manuscript. LS: design of the work and interpretation of data. JA: contributed materials / reagents /analysis tools. CZ and QM: design and revise the manuscript. All authors read and approved the final manuscript.

Funding This study was supported by National Natural Science Foundation of China (grant number 81972280, to Ming Quan); Natural Science Foundation of Shanghai Municipality (grant number 23ZR1452300, to Ming Quan); Academic Leaders Training Program of Pudong Health Bureau of Shanghai (grant number PWRd2022-02, to Ming Quan); Public Institutions Livelihood Research Project of Science and Technology Development Foundation of Pudong (grant number PKJ2023-Y37, to Zhiqin Chen).

Data availability No datasets were generated or analysed during the current study.

Declarations

Competing interests The authors declare no competing interests.

References

1. A. Vincent, J. Herman, R. Schulick et al., Pancreat. cancer Lancet. **378**(9791), 607–620 (2011)
2. R.L. Siegel, K.D. Miller, N.S. Wagle et al., Cancer statistics, 2023. CA Cancer J. Clin. **73**(1), 17–48 (2023)

3. J.J. Kim, I.F. Tannock, Repopulation of cancer cells during therapy: an important cause of treatment failure. Nat. Rev. Cancer. **5**(7), 516–525 (2005)
4. J. Ma, J. Cheng, Y. Gong et al., Downregulation of wnt signaling by sonic hedgehog activation promotes repopulation of human tumor cell lines. Dis. Model. Mech. **8**(4), 385–391 (2015)
5. J. Cheng, L. Tian, J. Ma et al., Dying tumor cells stimulate proliferation of living tumor cells via caspase-dependent protein kinase Cδ activation in pancreatic ductal adenocarcinoma. Mol. Oncol. **9**(1), 105–114 (2015)
6. C. Fang, C.Y. Dai, Z. Mei et al., microRNA-193a stimulates pancreatic cancer cell repopulation and metastasis through modulating TGF-β2/TGF-βRIII signalings. J. Exp. Clin. Cancer Res. **37**(1), 25 (2018)
7. Q. Huang, F. Li, X. Liu et al., Caspase 3-mediated stimulation of tumor cell repopulation during cancer radiotherapy. Nat. Med. **17**(7), 860–866 (2011)
8. T. Guo, Y. Lu, P. Li et al., A novel partner of Scalloped regulates Hippo signaling via antagonizing scalloped-yorkie activity. Cell. Res. **23**(10), 1201–1214 (2013)
9. L.M. Koontz, Y. Liu-Chittenden, F. Yin et al., The Hippo effector yorkie controls normal tissue growth by antagonizing scalloped-mediated default repression. Dev. Cell. **25**(4), 388–401 (2013)
10. M. Takai, S. Mori, K. Honoki et al., Roles of lysophosphatidic acid (LPA) receptor-mediated signaling in cancer cell biology. J. Bioenerg Biomembr. **56**(4), 475–482 (2024)
11. M. Quan, J.J. Cui, X. Feng et al., The critical role and potential target of the autotaxin/lysophosphatidate axis in pancreatic cancer. Tumour Biol. **39**(3), 1010428317694544 (2017)
12. F.X. Yu, B. Zhao, N. Panupinthu et al., Regulation of the Hippo-YAP pathway by G-protein-coupled receptor signaling. Cell. **150**(4), 780–791 (2012)
13. X. Zhao, D. Wang, Z. Zhao et al., Caspase-3-dependent activation of calcium-independent phospholipase A2 enhances cell migration in non-apoptotic ovarian cancer cells. J. Biol. Chem. **281**(39), 29357–29368 (2006)
14. J. Dong, G. Feldmann, J. Huang et al., Elucidation of a universal size-control mechanism in Drosophila and mammals. Cell. **130**(6), 1120–1133 (2007)
15. E. Mini, S. Nobili, B. Caciagli et al., Cellular pharmacology of gemcitabine. Ann. Oncol. **17**(Suppl 5), v7–12 (2006)
16. A. Ianevski, A.K. Giri, T. Aittokallio, SynergyFinder 3.0: an interactive analysis and consensus interpretation of multi-drug synergies across multiple samples. Nucleic Acids Res. **50**(W1), W739–w43 (2022)
17. M. Li, X. Rao, Y. Cui et al., The keratin 17/YAP/IL6 axis contributes to E-cadherin loss and aggressiveness of diffuse gastric cancer. Oncogene. **41**(6), 770–781 (2022)
18. C. Li, H. Zheng, J. Xiong et al., Mir-596-3p suppresses brain metastasis of non-small cell lung cancer by modulating YAP1 and IL-8. Cell. Death Dis. **13**(8), 699 (2022)
19. M.S. Brown, A. Radhakrishnan, J.L. Goldstein, Retrospective on cholesterol homeostasis: the Central Role of Scap. Annu. Rev. Biochem. **87**, 783–807 (2018)
20. B. Huang, B.L. Song, C. Xu, Cholesterol metabolism in cancer: mechanisms and therapeutic opportunities. Nat. Metab. **2**(2), 132–141 (2020)
21. R.J. King, P.K. Singh, K. Mehla, The cholesterol pathway: impact on immunity and cancer. Trends Immunol. **43**(1), 78–92 (2022)
22. A.P. Klein, Pancreatic cancer epidemiology: understanding the role of lifestyle and inherited risk factors. Nat. Rev. Gastroenterol. Hepatol. **18**(7), 493–502 (2021)
23. T. Conroy, P. Hammel, M. Hebbar et al., FOLFIRINOX or gemcitabine as adjuvant therapy for pancreatic cancer. N Engl. J. Med. **379**(25), 2395–2406 (2018)
24. S. Pusceddu, M. Ghidini, M. Torchio et al., Comparative effectiveness of gemcitabine plus nab-Paclitaxel and FOLFIRINOX in the first-line setting of metastatic pancreatic cancer: a systematic review and meta-analysis. Cancers (Basel). **11**(4) (2019)
25. Y. Li, S. Tang, X. Shi et al., Metabolic classification suggests the GLUT1/ALDOB/G6PD axis as a therapeutic target in chemotherapy-resistant pancreatic cancer. Cell. Rep. Med. **4**(9), 101162 (2023)
26. F. Baenke, B. Peck, H. Miess et al., Hooked on fat: the role of lipid synthesis in cancer metabolism and tumour development. Dis. Model. Mech. **6**(6), 1353–1363 (2013)
27. A.F. Hermens, G.W. Barendsen, Changes of cell proliferation characteristics in a rat rhabdomyosarcoma before and after x-irradiation. Eur J Cancer (1965). **5**(2), 173–89 (1969)
28. M.J. Jiang, Y.Y. Chen, J.J. Dai et al., Dying tumor cell-derived exosomal mir-194-5p potentiates survival and repopulation of tumor repopulating cells upon radiotherapy in pancreatic cancer. Mol. Cancer. **19**(1), 68 (2020)
29. L.M. Butler, Y. Perone, J. Dehairs et al., Lipids and cancer: emerging roles in pathogenesis, diagnosis and therapeutic intervention. Adv. Drug Deliv Rev. **159**, 245–293 (2020)
30. U. Bruning, F. Morales-Rodriguez, J. Kalucka et al., Impairment of angiogenesis by fatty acid synthase inhibition involves mTOR malonylation. Cell. Metab. **28**(6), 866–80.e15 (2018)
31. S. Tadros, S.K. Shukla, R.J. King et al., De Novo lipid synthesis facilitates Gemcitabine Resistance through endoplasmic reticulum stress in pancreatic Cancer. Cancer Res. **77**(20), 5503–5517 (2017)
32. R.B. Rawson, The SREBP pathway–insights from Insigs and insects. Nat. Rev. Mol. Cell. Biol. **4**(8), 631–640 (2003)
33. J. Luo, H. Yang, B.L. Song, Mechanisms and regulation of cholesterol homeostasis. Nat. Rev. Mol. Cell. Biol. **21**(4), 225–245 (2020)
34. W.H. Moolenaar, A. Perrakis, Insights into autotaxin: how to produce and present a lipid mediator. Nat. Rev. Mol. Cell. Biol. **12**(10), 674–679 (2011)
35. J.B. Park, C.S. Lee, J.H. Jang et al., Phospholipase signalling networks in cancer. Nat. Rev. Cancer. **12**(11), 782–792 (2012)
36. C. Laface, A.D. Ricci, S. Vallarelli et al., Autotaxin-Lysophosphatidate axis: promoter of cancer development and possible therapeutic implications. Int. J. Mol. Sci. **25**(14) (2024)
37. M.A. Dacheux, D.D. Norman, TIGYI G J et al., Emerging roles of lysophosphatidic acid receptor subtype 5 (LPAR5) in inflammatory diseases and cancer. Pharmacol. Ther. **245**, 108414 (2023)
38. J. Chen, H. Li, W. Xu et al., Evaluation of serum ATX and LPA as potential diagnostic biomarkers in patients with pancreatic cancer. BMC Gastroenterol. **21**(1), 58 (2021)
39. S. Ma, Z. Meng, R. Chen et al., The Hippo Pathway: Biology and Pathophysiology. Annu. Rev. Biochem. **88**, 577–604 (2019)
40. A. Kumar, B. Bharathwajchetty, M.K. Manickasamy et al., Natural compounds targeting YAP/TAZ axis in cancer: current state of art and challenges. Pharmacol. Res. **203**, 107167 (2024)
41. D. Xie, J. Cui, T. Xia et al., Hippo transducer TAZ promotes epithelial mesenchymal transition and supports pancreatic cancer progression. Oncotarget. **6**(34), 35949–35963 (2015)
42. B. Zhao, X. Wei, W. Li et al., Inactivation of YAP oncoprotein by the Hippo pathway is involved in cell contact inhibition and tissue growth control. Genes Dev. **21**(21), 2747–2761 (2007)
43. H. Kanda, R. Newton, R. Klein et al., Autotaxin, an ectoenzyme that produces lysophosphatidic acid, promotes the entry of lymphocytes into secondary lymphoid organs. Nat. Immunol. **9**(4), 415–423 (2008)
44. D.V. Krysko, P. Vandenabeele, From regulation of dying cell engulfment to development of anti-cancer therapy. Cell. Death Differ. **15**(1), 29–38 (2008)

45. K. Chen, Q. Wang, X. Liu et al., Immune profiling and prognostic model of pancreatic cancer using quantitative pathology and single-cell RNA sequencing. J. Transl Med. **21**(1), 210 (2023)
46. D.T. Chen, A.H. Davis-Yadley, P.Y. Huang et al., Prognostic Fifteen-Gene signature for early stage pancreatic ductal adenocarcinoma. PLoS One. **10**(8), e0133562 (2015)